# Repair concrete structures with high-early-strength engineered cementitious composites (HES-ECC)

## Material design and interfacial behavior

Jiang, Bo; Qian, Zhenxu; Gu, Dawei; Pan, Jinlong

**DOI**
10.1016/j.jobe.2023.106060

**Publication date**
2023

**Document Version**
Final published version

**Published in**
Journal of Building Engineering

**Citation (APA)**
Jiang, B., Qian, Z., Gu, D., & Pan, J. (2023). Repair concrete structures with high-early-strength engineered cementitious composites (HES-ECC): Material design and interfacial behavior. *Journal of Building Engineering*, *68*, Article 106060. https://doi.org/10.1016/j.jobe.2023.106060

Journal of Building Engineering 68 (2023) 106060

Contents lists available at ScienceDirect

Journal of Building Engineering

journal homepage: www.elsevier.com/locate/jobe

# Repair concrete structures with high-early-strength engineered cementitious composites (HES-ECC): Material design and interfacial behavior

Bo Jiang [a], Zhenxu Qian [a, b], Dawei Gu [a, b], Jinlong Pan [a, *]

[a] Key Laboratory of Concrete and Prestressed Concrete Structures of Ministry of Education, School of Civil Engineering, Southeast University, Nanjing, 211189, PR China

[b] Faculty of Civil Engineering and Geosciences, Delft University of Technology, 2628 CN, Delft, the Netherlands

ARTICLE INFO

*Keywords:*
ECC
High-early-strength
Interfacial behavior
Deformability

ABSTRACT

Aimed at realizing the effective strengthening and durable repair of concrete structures, particularly in emergencies like traffic interruption triggered by broken roads and damaged bridges, nine groups of specimens were designed and tested in this paper to develop the high-early-strength Engineered Cementitious Composites (HES-ECC) featured as both high early-strength and superior long-term-deformability. The high-early-strength effect of sulphoaluminate cement, silica fume, and Portland cement on HES-ECC was compared, as well as their influence on the deformation ability of HES-ECC. Moreover, the interfacial behaviors between HES-ECC and existing concrete structure were clarified, considering the effects of interfacial agents, interfacial treatment methods, and interfacial roughness. The results indicate that HES-ECC with 6% silica fume mixed could obtain both the high early-strength and superior long-term-deformability. The flexural strength at 3 h could reach 66.67% of that at 28d. The compressive strength could reach up to 28.7 MPa at 3 h, and the ultimate tensile strain could remain 4.21% at 28d. Cement paste interfacial agent could enhance the chemical adhesive bonding between HES-ECC and existing concrete while polymer modified interfacial agent was incompatible. The increased roughness of chiseled interface was beneficial to both the bearing capacity and the deformation ability. Interfacial shear performance of the grooved interface was scarcely deteriorated even if the roughness decreased by 54.18% compared with the chiseled interface. The recommended interfacial treatment is chiseled interface combined with grooved interface, as well as a thickness of 1–2 mm cement paste interfacial agent. This study provides valuable and credible experimental data for promoting the application of HES-ECC in repairing existing concrete structures in practice.

## 1. Introduction

Structural concrete has been used for construction widely due to its superior mechanical performance but low cost. However, lack of durability has become a challenging problem for conventional concrete under severe serving conditions like fatigue, impact, freeze-thaw cycles, chloride penetration, etc. Effective strengthening and durable repair are often required to reduce the lifecycle cost and prolong the service life of existing concrete structures [1–4]. Common repair materials for the concrete structures can be classified into pure cement-based materials (Portland cement, magnesium phosphate cement, high alumina cement, etc.), polymer modi-

* Corresponding author.
*E-mail address:* cejlpan@seu.edu.cn (J. Pan).

https://doi.org/10.1016/j.jobe.2023.106060
Received 18 November 2022; Received in revised form 12 January 2023; Accepted 5 February 2023
Available online 10 February 2023

fied cement-based materials (styrene-butadiene rubber (SBR) latex modified, acrylic and some vinyl copolymers modified, etc.), and pure polymers (epoxy resin, polyester, polyurethane, etc.) as a whole [5]. Unfortunately, it is estimated that more than half of concrete repairs end in failure, of which three-quarters result from the absence of durability of the repair materials [6,7]. Cement in repair materials could lead to the change of interfacial microstructure and the increase of interfacial drying shrinkage stress. It further resulted in the cracking and debonding of the repair layers [8,9]. Regarding polymer in repair materials, for instance, resin was found to react with the cement by Sasse and Fiebrich [10]. The durability of repair materials was weakened in such a situation with the increased alkalinity and the softened resin.

Engineered Cementitious Composites (ECC) with characteristics of multiple-cracking and strain-hardening has been regarded as an ideal material for strengthening and repair [11]. It was introduced to overcome the brittle fracture and poor durability of conventional cementitious materials based on the fracture mechanics, statistics, and micromechanics. Both strength criterion and energy criterion should be considered during the design process of ECC [12,13]. It has a superior ability of deformation and crack-controlling. The ultimate tensile strain can steadily reach over 3% and the crack width is controlled under 60–100 μm at the limit state, improving the durability of ECC in harsh environments such as resistance to penetration of corrosive substances [14]. Besides, sufficient deformability also helps to enhance the composite effect between ECC repair layer and existing concrete structures. Meanwhile, it further guarantees the load-bearing capacity and improves the ductility of the integral structure after repair [15,16].

Given the outstanding mechanical properties and durability of ECC, considerable efforts have been devoted to investigating its applicability as repair materials. And the interfacial behaviors between ECC and existing concrete is one of the key issues. The influence of loading conditions, strength of ECC, interfacial treatment methods, interfacial roughness, interfacial agents, construction technologies, etc. is taken into account [7,17–26]. It was found that the interfacial roughness had a marked impact on the interfacial behaviors between ECC and concrete. The calculation method of nominal interfacial strength and the evaluation criteria of failure mode were proposed [17,18]. Besides, suitable interfacial agents could also help to fill in the voids of the existing concrete and improve the microstructure of interface [7,19]. The degradation of interfacial behaviors under harsh environments was also considered such as high temperature, freeze-thaw cycles, sulfate attack, etc. The interfacial shear strength increased with temperature below 400 °C while decreased with increasing temperature above 400 °C [23]. Salt freeze-thaw erosion had a very negative effect on the interfacial fracture performance, including initial crack stage, stable crack propagation stage, and instability failure stage [25]. Compared with the failure of concrete/concrete interface after 60 sulfate and wet-dry cycles, the corrosion resistance coefficient of ECC/concrete interface remained above 60% even after 120 cycles [26].

In addition to the desirable interfacial behaviors, strength development during the early age is also essential for repair materials, especially for the application in emergencies such as road repair and bridge strengthening, which are closely associated with the economic benefits and social impacts. ECC with high-early-strength can provide sufficient strength instantly and extend the maintenance interval remarkably at the same time [6]. Medium-early-strength ECC (MES-ECC) featured as self-healing was developed by adding accelerator to ordinary Portland cement, with compressive strength reaching 24 MPa at age 3 d [27]. Wang and Li [6,28] proposed two systems of high-early-strength ECC (HES-ECC) with proprietary rapid-hardening cement and Type III Portland cement, respectively, in which artificial flaws were introduced to guarantee the long-term deformability. HES-ECC with proprietary rapid-hardening cement obtained 24 MPa within 3 h after casting, and the long-term tensile strain was greater than 2.0%. The compressive strength of HES-ECC produced by Type III Portland cement and calcium nitrate-based accelerator could reach 21 MPa within 4 h, and the long-term tensile strain was greater than 3.0%. Besides, according to the research of Şahmaran et al. [29], the compressive strength of HES-ECC was tested to be 20 MPa within 6 h by applying high-early-strength Portland cement and calcium nitrate-based accelerator, while the combination of sulphoaluminate cement and silica fume was reported as 25 MPa within 6 h in Ref. [30]. However, the ultimate tensile strain was limited to merely 1.8% [30]. HES-ECC produced by proprietary rapid-hardening cement without artificial flaws obtained an ultimate tensile strain over 6% at the age of 7 h, but it reduced to 0.7% at the age of 3d inversely [6]. Similarly, that of HES-ECC produced by Type III Portland cement without artificial flaws was slightly higher than 1.0% at 28d [6]. HES-ECC in current researches can hardly obtain both high early-strength and superior long-term-deformability. Deterioration of deformation ability and disappearance of multiple-cracking can result in severe adverse repair effects. The durability of HES-ECC repair layer is weakened and the safety of the integral structure is decreased.

Thus, as to HES-ECC, it is essential to ensure the high-early-strength as well as the long-term ability of deformation and crack-controlling. Moreover, desirable interfacial behaviors between HES-ECC and existing concrete structures are also need to be provided. But few relevant studies have been conducted. Yildirim et al. [29,31] studied the interfacial behaviors between HES-ECC and concrete through direct tension and slant shear tests, taking the influence of compressive strength and self-shrinkage of HES-ECC into consideration. But the interfacial treatment methods, interfacial agents, and some other factors were not involved. Thus, aimed at proposing a kind of HES-ECC featured as both high early-strength and superior long-term-deformability, the high-early-strength effect of sulphoaluminate cement, silica fume, and Portland cement on HES-ECC was compared. And their influence on the deformation ability of HES-ECC was studied at the same time. On this basis, the interfacial behavior tests between HES-ECC and existing concrete were further carried out to choose the optimal interfacial agents, interfacial treatment methods, and interfacial roughness. It provides useful references and suggestions for the design and construction of HES-ECC as repair materials for existing concrete structures in practice.

## 2. Experimental program

### 2.1. Materials and mixtures

Raw materials within the mixtures of HES-ECC include L●SAC425 low-alkali sulphoaluminate cement (SAC), Class II fly ash (FA), silica fume (SF), P●II425R Portland cement (PC), 80–100 mesh quartz sand, water, solid citric acid, PCA®-VIII polycarboxylate-series

superplasticizer (SP), and polyvinyl-alcohol fiber (PVA, the length is 12 mm, the diameter is 38 μm, the elastic modulus is 42.8 GPa, and the tensile strength is 1620 MPa). Chemical compositions of raw materials can be found in Table 1, and detailed mixture proportions of HES-ECC are listed in Table 2. Mixture A3S0P0 was taken as the controlled group, and the influence of the mass ratio between SAC and FA (SAC/FA ratio) and the addition of SF and PC were studied. Given the early-strength and long-term-deformability of HES-ECC, A3S6P0 was selected as the optimal mixture to further test the interfacial behaviors between HES-ECC and concrete. River sand with fineness modulus 2.18 and coarse aggregate with maximum particle size less than 16 mm were used for preparing the existing concrete in the interfacial bond tests. Two types of interfacial agents were prepared, namely cement paste interfacial agent and polymer (SBR latex with solid content 50%) modified interfacial agent (Table 3). The cubic compressive strength of concrete, cement paste interfacial agent, and polymer modified interfacial agent was tested to be 41.8 MPa, 41.5 MPa, and 29.4 MPa at testing age 3 h in the interfacial bond tests, separately, which further increased up to 46.3 MPa, 61.4 MPa, and 60.1 MPa at testing age 28d.

### 2.2. Specimen preparation

Specimens for the flexure, compression, and uniaxial tension tests were cast following the similar procedure in Ref. [32]. For the interfacial bond tests, specimens were fabricated by four steps as shown in Fig. 1: (i) concrete substrate was cast and cured until 28d; (ii) then, one of the side surfaces of the concrete substrate, regarding as the interface, was chiseled or grooved (Fig. 2); (iii) after wetting the interface repeatedly, the interfacial agent was brushed with a thickness of 1–2 mm; (iv) finally, HES-ECC side was poured, and the composite specimens were cured till the testing ages. All specimens were cured under temperature 20 ± 2 °C and relative humidity 95 ± 5%, following the Chinese Standard GB/T 50081 [33]. To measure the interfacial roughness, so-called "sand filling method" was applied [23]. Specifically, the interface was covered with standard sand to the same height as the highest point of the interface, and the mass of sand was measured. Converted into volume and divided by cross-sectional area, the roughness coefficient of interface was then obtained.

The testing ages 3 h, 6 h, 1d, 7d, and 28d counting from adding water to the dry binder when mixing HES-ECC are labeled as A-E, respectively. With gradual increase of the interfacial roughness, the chiseled interfaces are labeled as I, II, III, while the roughness grade IV corresponded to the grooved interface (Fig. 2). Specimens for interfacial bond tests are named as "T/V–N/P/S-X-Y", among which the first letter "T" represents the splitting tests while "V" represents the direct shear tests. The second letter "N", "P", "S" represents no interfacial agent, cement paste interfacial agent, and polymer modified interfacial agent, respectively. The suffix "X" represents the type of interface and "Y" denotes the testing age. Detailed roughness coefficient of specimens for interfacial bond tests are listed in Tables 6 and 7.

**Table 1**
Chemical compositions of raw materials (by mass, %).

| Raw materials | CaO | $SO_3$ | $Al_2O_3$ | $SiO_2$ | $Fe_2O_3$ | $TiO_2$ | MgO | $K_2O$ | LOI |
|---|---|---|---|---|---|---|---|---|---|
| SAC | 55.13 | 16.66 | 16.37 | 5.96 | 2.41 | 1.15 | 0.77 | 0.73 | 0.82 |
| FA | 4.89 | 0.63 | 43.85 | 41.28 | 4.77 | 1.65 | 1.20 | 0.72 | 1.01 |
| SF | 0.45 | 1.08 | 0.13 | 96.35 | 0.06 | / | 0.35 | 0.89 | 0.68 |
| PC | 64.16 | 2.33 | 5.86 | 20.65 | 3.56 | 0.27 | 1.42 | 1.27 | 0.48 |

**Table 2**
Mixture proportions of HES-ECC (by mass).

| No. | SAC | FA | SF | PC | Quartz sand | Water | Citric acid/C[a] (%) | SP/C (%) | Fiber volume ratio (%) | SAC/FA | SF/C (%) | PC/C (%) |
|---|---|---|---|---|---|---|---|---|---|---|---|---|
| A2S0P0 | 0.667 | 0.333 | 0.00 | 0.00 | 0.35 | 0.32 | 0.12 | 0.81 | 2.0 | 2 | 0 | 0 |
| A3S0P0 | 0.750 | 0.250 | 0.00 | 0.00 | 0.35 | 0.32 | 0.12 | 0.81 | 2.0 | 3 | 0 | 0 |
| A4S0P0 | 0.800 | 0.200 | 0.00 | 0.00 | 0.35 | 0.32 | 0.12 | 0.81 | 2.0 | 4 | 0 | 0 |
| A3S2P0 | 0.735 | 0.245 | 0.02 | 0.00 | 0.35 | 0.32 | 0.12 | 0.81 | 2.0 | 3 | 2 | 0 |
| A3S4P0 | 0.720 | 0.240 | 0.04 | 0.00 | 0.35 | 0.32 | 0.12 | 0.81 | 2.0 | 3 | 4 | 0 |
| A3S6P0 | 0.705 | 0.235 | 0.06 | 0.00 | 0.35 | 0.32 | 0.12 | 0.81 | 2.0 | 3 | 6 | 0 |
| A3S0P4 | 0.720 | 0.240 | 0.00 | 0.04 | 0.35 | 0.32 | 0.12 | 0.81 | 2.0 | 3 | 0 | 4 |
| A3S0P8 | 0.690 | 0.230 | 0.00 | 0.08 | 0.35 | 0.32 | 0.12 | 0.81 | 2.0 | 3 | 0 | 8 |
| A3S0P12 | 0.660 | 0.220 | 0.00 | 0.12 | 0.35 | 0.32 | 0.12 | 0.81 | 2.0 | 3 | 0 | 12 |

[a] C represents the binder, which contains SAC, FA, SF, and PC in HES-ECC.

**Table 3**
Proportions of other mixtures in the interfacial bond tests (by mass).

| Mixture | Water | PC | SAC | River sand | Coarse aggregate | SP/C[a] (%) | SBR latex | Defoamer |
|---|---|---|---|---|---|---|---|---|
| Concrete | 0.38 | 1.00 | / | 0.76 | 1.48 | 0.13 | / | / |
| Cement paste interfacial agent | 0.28 | / | 1.00 | / | / | 0.92 | / | / |
| Polymer modified interfacial agent | 0.21 | / | 1.00 | / | / | / | 0.15 | 0.0012 |

[a] C represents the binder, which contains PC in concrete and SAC in cement paste interfacial agent.


**Fig. 1.** Casting process of specimens for (a) splitting tests (b) direct shear tests.

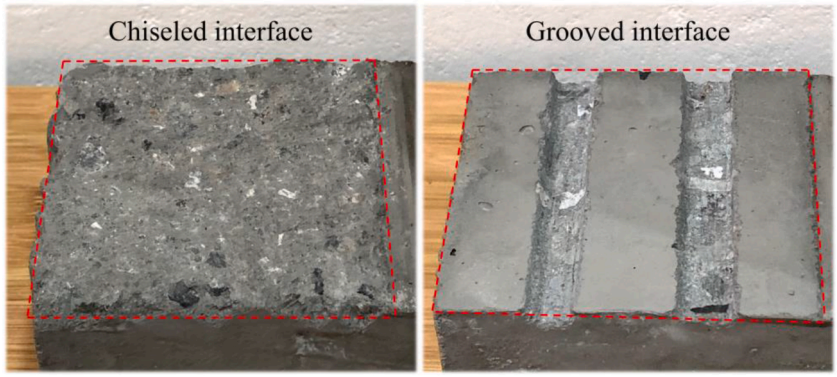


**Fig. 2.** Different types of interface.

### 2.3. Test methods

#### 2.3.1. Flexure and compression tests

Three-point bending tests of prisms (160 mm × 40 mm × 40 mm) were conducted to test the flexural strength of HES-ECC following the Chinese Standard GB/T 17671–1999 (idt ISO 679:1989) [34]. The flexural strength is calculated by $\sigma_f = 1.5F_f L/b^3$, where $F_f$ is the load applied at midspan, $L$ is the distance between the bottom supports (100 mm), and $b$ is the width (40 mm). Cubic specimens (70.7 mm × 70.7 mm × 70.7 mm) were used for compression tests of HES-ECC following the Chinese Standard JGJ/T 70 [35]. For both flexure and compression tests, three specimens were tested at the ages of 3 h, 6 h, 1d, 7d, and 28d for each group.

#### 2.3.2. Uniaxial tension tests

The standard dumbbell-shaped specimens (Fig. 3(a)) were prepared for testing the uniaxial tension behaviors of HES-ECC, following the recommendations of Japan Society of Civil Engineers (JSCE) [36]. Considering the limited testing time during the early stage, four dumbbell-shaped specimens in one group were tested at ages 3 h and 1d, while six specimens were tested at age 28d. The electronic universal testing machine (10 kN) was used to apply the uniaxial tensile load, and two linear variable displacement transducers (LVDTs) were installed on both sides of the specimen to measure the tensile deformation with a gauge length of 80 mm (Fig. 3(b)).

#### 2.3.3. Interfacial splitting tests

The specimen size and the testing scheme of interfacial splitting tests are illustrated in Fig. 3(c). Four composite cubic specimens with a size of 150 mm × 150 mm × 150 mm were tested under uniaxial compression at the ages of 3 h and 28d. The load was applied by a 300 kN electronic universal testing machine with a loading speed of 0.5 kN/s. By incorporating an arc-shaped steel block and adjusting the position of the specimen, the vertical stress-bearing surface was ought to be the interface between HES-ECC and concrete. To reduce the stress concentration, two pieces of plywood (150 mm × 20 mm × 4 mm) were placed between the steel block and the specimen. The splitting tensile strength is then calculated by $\sigma_t = 2F_t/\pi A$, where $F_t$ is the applied load, and $A$ is the cross-sectional area (150 × 150 mm$^2$).

#### 2.3.4. Interfacial direct shear tests

A type of Z-shaped specimen [23] (Fig. 3(d)) was adopted for the interfacial direct shear tests. Three specimens were tested under uniaxial compression with a loading speed of 0.5 kN/min by the same machine used in the splitting tests after curing for 28d. An arc-

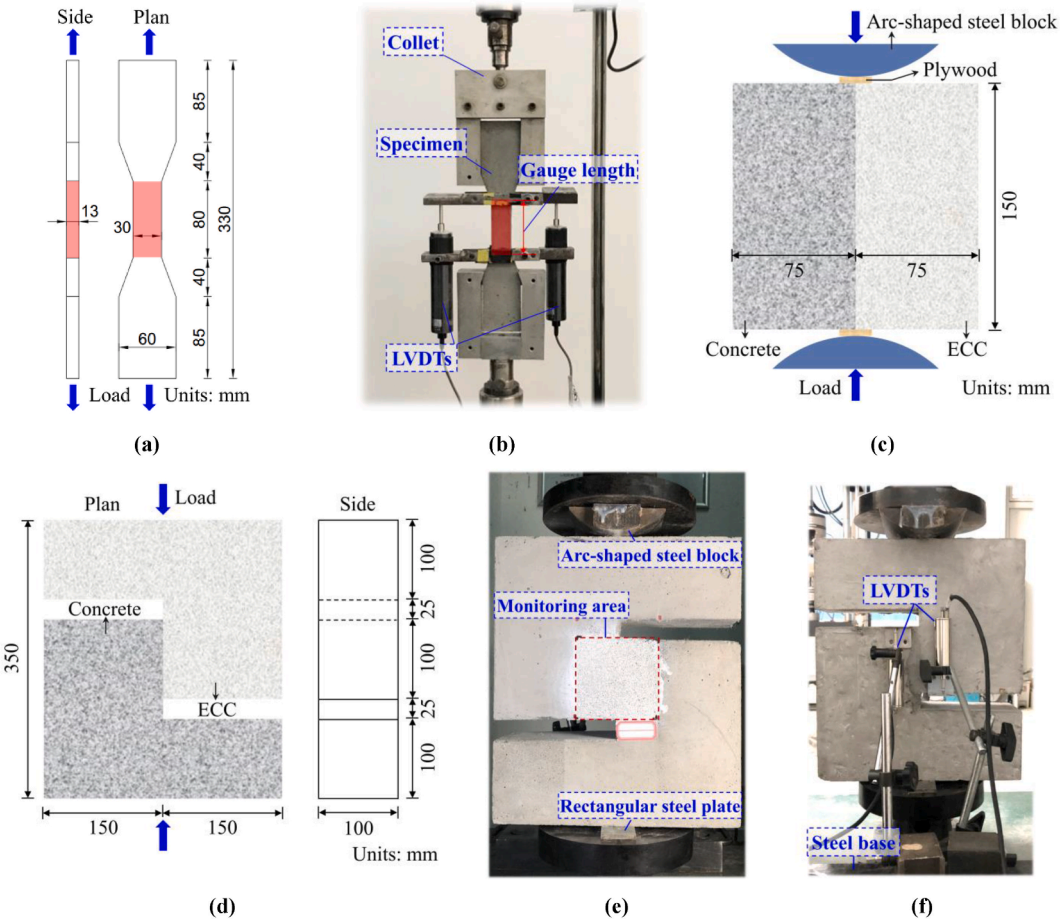


**Fig. 3.** Specimens and testing instruments (a) dumbbell-shaped specimen (b) sketch of the instrument for uniaxial tension tests (c) sketch of the instrument for splitting tests (d) Z-shaped specimen (e) the front of the instrument for direct shear tests (f) the backside of the instrument for direct shear tests.

shaped steel block was placed above the specimen, along with a 40 mm wide steel block setting underneath, as shown in Fig. 3(e). To capture the deformation and the crack propagation within the interfacial zones, the Digital Image Correlation (DIC) system was equipped. Two LVDTs were installed on the backside of the specimen to measure the relative slip of the interface (Fig. 3(f)). The interfacial shear strength $\sigma_s$ is then calculated by dividing the shear load by the cross-sectional area of the interface (100 × 100 mm$^2$).

## 3. Test results and discussion

### 3.1. Flexure and compression tests

The average value and the standard deviation of the flexural and compressive strength of HES-ECC are listed in Table 4 and Table 5, as well as the strength growing rate between adjacent testing ages. Influence of SAC/FA ratio, SF, and PC on the flexural and compressive strength of HES-ECC at different testing ages are illustrated in Figs. 4 and 5. The flexural and compressive strength of all groups increased with age.

#### 3.1.1. Effect of SAC/FA ratio

As the dominant cementitious component in this research, SAC features fast hydration and high early-strength [37], which can greatly influence the mechanical behaviors of HES-ECC as repair material. Despite the sustaining flexural strength growth of A2S0P0, A3S0P0 and A4S0P0 over time, the strength growth from 3 h to 6 h was most evident compared with other intervals regardless of the SAC/FA ratio. And A4S0P0 reached the peak as 34.02%. Furthermore, the HES-ECC tended to have a higher flexural strength with the increase of SAC/FA ratio. At age 28d, the flexural strength of A3S0P0 and A4S0P0 increased by 10.06% and 13.21% compared with A2S0P0, separately, with SAC/FA ratio rising from 2.0 to 3.0 and 4.0. This is owing to the slow hydration characteristics of FA, which are completely contrary to SAC [38]. The increased SAC/FA ratio obtains a higher hydration rate of the binder, which densifies the matrix and also enhances the bonding between fibers and matrix [37].

A similar tendency can be found in the compressive strength of HES-ECC when increasing SAC/FA ratio. The compressive strength of A3S0P0 and A4S0P0 was 3.72% and 6.20% higher than that of A2S0P0 at age 3 h, and was 3.73% and 9.68% higher at age 28d. Be-

**Table 4**
Flexural strength of HES-ECC at different testing ages (MPa).

| No. | 3 h (A) | 6 h (B) | | 1d (C) | | 7d (D) | | 28d (E) | |
|---|---|---|---|---|---|---|---|---|---|
| | AVE (SD)[a] | IR | AVE (SD) | IR | AVE (SD) | IR | AVE (SD) | IR | AVE (SD) |
| A2S0P0 | 9.1 (1.12) | 32.97% | 12.1 (0.53) | 7.44% | 13.0 (0.74) | 9.23% | 14.2 (1.07) | 11.97% | 15.9 (1.06) |
| A3S0P0 | 9.5 (0.68) | 33.68% | 12.7 (0.92) | 8.66% | 13.8 (0.74) | 13.04% | 15.6 (1.10) | 12.18% | 17.5 (0.70) |
| A4S0P0 | 9.7 (0.63) | 34.02% | 13.0 (0.91) | 11.54% | 14.5 (1.20) | 8.97% | 15.8 (0.85) | 13.92% | 18.0 (0.74) |
| A3S2P0 | 11.2 (0.96) | 15.18% | 12.9 (0.76) | 8.53% | 14.0 (0.47) | 14.29% | 16.0 (1.07) | 10.63% | 17.7 (1.21) |
| A3S4P0 | 12.4 (0.77) | 10.48% | 13.7 (1.56) | 10.95% | 15.2 (0.79) | 10.53% | 16.8 (1.16) | 11.90% | 18.8 (1.90) |
| A3S6P0 | 12.6 (1.08) | 16.67% | 14.7 (1.22) | 4.76% | 15.4 (0.82) | 10.39% | 17.0 (0.79) | 11.18% | 18.9 (1.63) |
| A3S0P4 | 11.8 (0.94) | 16.10% | 13.7 (1.43) | 2.92% | 14.1 (0.91) | 17.73% | 16.6 (1.14) | 7.23% | 17.8 (1.08) |
| A3S0P8 | 11.9 (0.53) | 18.49% | 14.1 (0.27) | 8.51% | 15.3 (0.34) | 9.80% | 16.8 (0.42) | 6.55% | 17.9 (1.32) |
| A3S0P12 | 12.1 (0.23) | 23.14% | 14.9 (0.67) | 4.03% | 15.5 (1.55) | 10.32% | 17.1 (0.86) | 8.19% | 18.5 (1.34) |

[a] AVE represents the average value. SD represents the standard deviation. IR represents the increasing rate between adjacent ages.

**Table 5**
Compressive strength of HES-ECC at different testing ages (MPa).

| No. | 3 h (A) | 6 h (B) | | 1d (C) | | 7d (D) | | 28d (E) | |
|---|---|---|---|---|---|---|---|---|---|
| | AVE (SD) | IR | AVE (SD) | IR | AVE (SD) | IR | AVE (SD) | IR | AVE (SD) |
| A2S0P0 | 24.2 (0.13) | 25.62% | 30.4 (0.91) | 13.16% | 34.4 (1.19) | 28.49% | 44.2 (1.15) | 21.49% | 53.7 (0.40) |
| A3S0P0 | 25.1 (0.12) | 30.68% | 32.8 (0.59) | 13.72% | 37.3 (2.68) | 24.93% | 46.6 (0.90) | 19.53% | 55.7 (0.49) |
| A4S0P0 | 25.7 (0.89) | 31.13% | 33.7 (0.71) | 21.36% | 40.9 (3.53) | 22.49% | 50.1 (1.44) | 17.56% | 58.9 (0.72) |
| A3S2P0 | 26.4 (1.28) | 30.68% | 34.5 (0.32) | 12.17% | 38.7 (1.22) | 23.00% | 47.6 (1.14) | 18.07% | 56.2 (1.27) |
| A3S4P0 | 27.6 (1.13) | 31.16% | 36.2 (1.11) | 11.05% | 40.2 (1.15) | 21.39% | 48.8 (0.97) | 17.01% | 57.1 (0.99) |
| A3S6P0 | 28.7 (1.26) | 32.06% | 37.9 (1.42) | 10.55% | 41.9 (0.50) | 18.62% | 49.7 (1.13) | 16.50% | 57.9 (0.79) |
| A3S0P4 | 26.0 (1.20) | 27.31% | 33.1 (1.22) | 11.48% | 36.9 (0.89) | 23.85% | 45.7 (1.39) | 19.47% | 54.6 (0.72) |
| A3S0P8 | 26.6 (0.64) | 25.19% | 33.3 (1.26) | 10.21% | 36.7 (2.90) | 21.25% | 44.5 (1.01) | 17.30% | 52.2 (1.29) |
| A3S0P12 | 27.9 (0.78) | 15.05% | 32.1 (1.68) | 13.40% | 36.4 (1.52) | 20.60% | 43.9 (1.31) | 16.63% | 51.2 (1.60) |

**Table 6**
Roughness and splitting tensile strength.

| No. | Roughness (mm) | | Splitting tensile strength (MPa) | | No. | Roughness (mm) | | Splitting tensile strength (MPa) | |
|---|---|---|---|---|---|---|---|---|---|
| TNIIA | 1.39 | AVE = 1.45 SD = 0.08 | 2.19 | AVE = 1.94 SD = 0.18 | TNIIE | 1.49 | AVE = 1.50 SD = 0.05 | 2.29 | AVE = 2.45 SD = 0.11 |
| | 1.56 | | 2.04 | | | 1.56 | | 2.53 | |
| | 1.49 | | 1.80 | | | 1.51 | | 2.41 | |
| | 1.35 | | 1.75 | | | 1.44 | | 2.57 | |
| TPIIA | 1.47 | AVE = 1.48 SD = 0.04 | 2.10 | AVE = 2.12 SD = 0.09 | TPIIE | 1.35 | AVE = 1.46 SD = 0.08 | 2.43 | AVE = 2.68 SD = 0.16 |
| | 1.44 | | 2.27 | | | 1.43 | | 2.86 | |
| | 1.55 | | 2.01 | | | 1.48 | | 2.74 | |
| | 1.48 | | 2.08 | | | 1.56 | | 2.69 | |
| TSIIA | 1.41 | AVE = 1.44 SD = 0.05 | 1.87 | AVE = 1.86 SD = 0.14 | TSIIE | 1.43 | AVE = 1.44 SD = 0.07 | 2.10 | AVE = 2.19 SD = 0.12 |
| | 1.52 | | 1.70 | | | 1.55 | | 2.36 | |
| | 1.39 | | 1.81 | | | 1.39 | | 2.24 | |
| | 1.44 | | 2.08 | | | 1.38 | | 2.06 | |

sides, a higher SAC/FA ratio resulted in the rise of increasing rate before 1d. The strength growth slowed down later, and the HES-ECC with the highest SAC/FA ratio even exhibited the lowest growing rate, reflecting the high-early-strength effect of SAC.

### *3.1.2. Effect of SF*

Addition of SF with high activity could remarkably increase the flexural strength of HES-ECC, especially the early-strength within 3 h after casting. The flexural strength at the age of 3 h was increased by 32.63% when substituting the binder (SAC and FA) with only 6% SF. Nevertheless, different from the controlled group A3S0P0, the strength growth from 3 h to 6 h was insignificant, and minor difference was found in the increasing rate among different testing intervals. The flexural strength of A3S2P0, A3S4P0 and A3S6P0 at age 3 h took up 63.28%, 65.96%, and 66.67% of that at age 28d, respectively, while that of A3S0P0 was merely 54.29%. At the following testing ages, the proportion of flexural strength of A3S0P0, A3S2P0, A3S4P0 and A3S6P0 compared with age 28d basically came to the same level, ranging from 72.57% to 77.78% at age 6 h, from 78.86% to 81.48% at age 1d, and from 89.14% to 90.40% at age 7d. From another perspective, in spite of a higher flexural strength generated by more SF at each age, the difference between A3S6P0 with most SF and A3S0P0 still decreased with age (3.1 MPa, 2.0 MPa, 1.6 MPa, 1.4 MPa, and 1.4 MPa at each testing age). However, compared with A2S0P0, A4S0P0 showed a persistent growth (0.6 MPa, 0.9 MPa, 1.5 MPa, 1.6 MPa, and 2.1 MPa at each testing age). As the mineral admixture, SF occupies only a small part in the cementitious system of HES-ECC. It can hardly bring

**Table 7**
Roughness, relative slip, shear stiffness, and shear strength in the interfacial direct shear tests.

| No. | Roughness (mm) | Relative slip (mm) | | | Shear stiffness (N•mm$^{-3}$) | Shear strength (MPa) |
|---|---|---|---|---|---|---|
| | | Upward | Flat | Total | | |
| VNIE | 0.50 AVE = 0.52 | 0.2747 AVE = 0.2745 | 0.0156 AVE = 0.0152 | 0.2903 AVE = 0.2896 | 85.55 AVE = 89.13 | 2.39 AVE = 2.50 |
| | 0.54 SD = 0.02 | 0.2988 SD = 0.0200 | 0.0137 SD = 0.0011 | 0.3125 SD = 0.0189 | 92.60 SD = 2.88 | 2.80 SD = 0.22 |
| | 0.52 | 0.2499 | 0.0162 | 0.2661 | 89.24 | 2.30 |
| VNIIE | 1.43 AVE = 1.48 | 0.3197 AVE = 0.3282 | 0.0132 AVE = 0.0245 | 0.3329 AVE = 0.3527 | 93.68 AVE = 94.43 | 3.04 AVE = 3.19 |
| | 1.48 SD = 0.04 | 0.3285 SD = 0.0069 | 0.0262 SD = 0.0086 | 0.3547 SD = 0.0154 | 91.87 SD = 2.45 | 3.15 SD = 0.15 |
| | 1.52 | 0.3365 | 0.0340 | 0.3705 | 97.74 | 3.39 |
| VNIIIE | 2.83 AVE = 2.75 | 0.3177 AVE = 0.3056 | 0.0746 AVE = 0.1011 | 0.3923 AVE = 0.4068 | 111.46 AVE = 108.09 | 3.80 AVE = 3.52 |
| | 2.77 SD = 0.07 | 0.2486 SD = 0.0425 | 0.1486 SD = 0.0336 | 0.3972 SD = 0.0171 | 123.45 SD = 14.12 | 3.37 SD = 0.20 |
| | 2.65 | 0.3506 | 0.0802 | 0.4308 | 89.36 | 3.38 |
| VNIVE | 1.26 AVE = 1.26 | 0.3345 AVE = 0.2953 | 0.0839 AVE = 0.1034 | 0.4184 AVE = 0.3986 | 92.80 AVE = 108.02 | 3.29 AVE = 3.45 |
| | 1.23 SD = 0.03 | 0.2763 SD = 0.0277 | 0.1024 SD = 0.0163 | 0.3787 SD = 0.0162 | 107.31 SD = 12.73 | 3.32 SD = 0.21 |
| | 1.30 | 0.2750 | 0.1238 | 0.3988 | 123.96 | 3.75 |
| VPIIE | 1.52 AVE = 1.46 | 0.3054 AVE = 0.2474 | 0.0202 AVE = 0.0408 | 0.3256 AVE = 0.2881 | 118.73 AVE = 139.42 | 3.70 AVE = 3.62 |
| | 1.39 SD = 0.05 | 0.2285 SD = 0.0419 | 0.0317 SD = 0.0215 | 0.2602 SD = 0.0275 | 131.77 SD = 20.74 | 3.26 SD = 0.27 |
| | 1.48 | 0.2082 | 0.0704 | 0.2786 | 167.77 | 3.91 |
| VSIIE | 1.34 AVE = 1.47 | 0.2584 AVE = 0.2479 | 0.0204 AVE = 0.0630 | 0.2788 AVE = 0.3108 | 79.76 AVE = 92.75 | 2.17 AVE = 2.50 |
| | 1.52 SD = 0.10 | 0.2837 SD = 0.0344 | 0.0378 SD = 0.0484 | 0.3215 SD = 0.0231 | 92.28 SD = 10.80 | 2.78 SD = 0.25 |
| | 1.56 | 0.2015 | 0.1307 | 0.3322 | 106.20 | 2.55 |

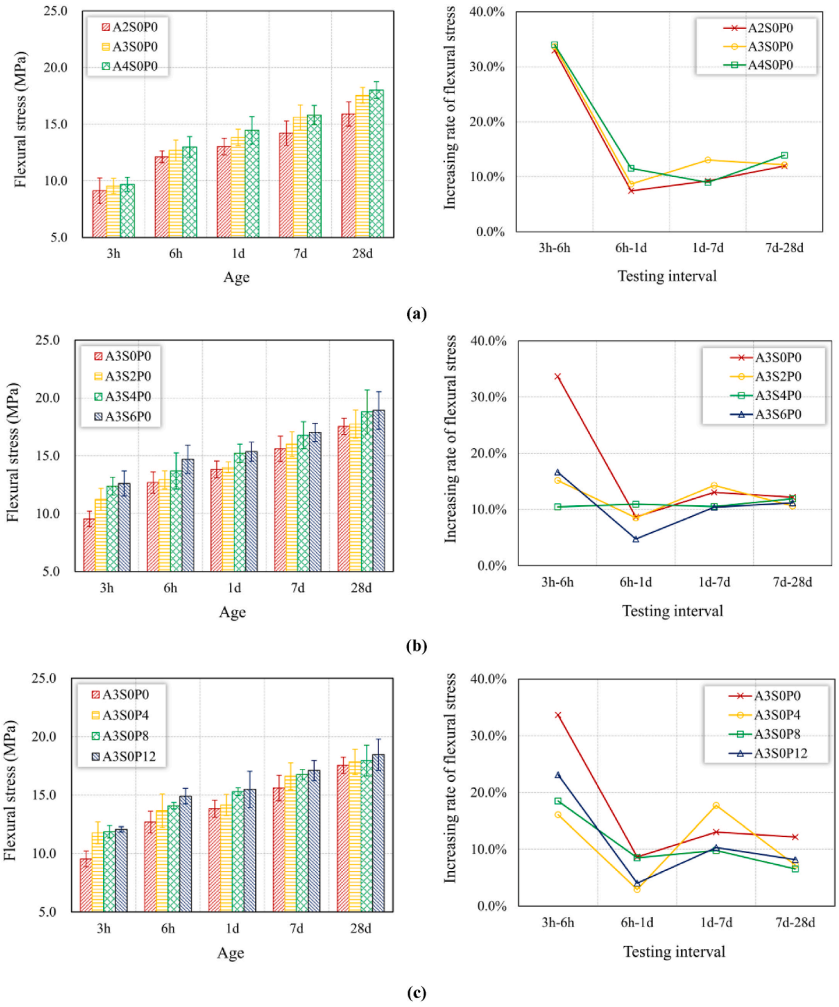


**Fig. 4.** Effects of different components on the flexural strength of HES-ECC with age (a) SAC/FA ratio (b) SF (c) PC.

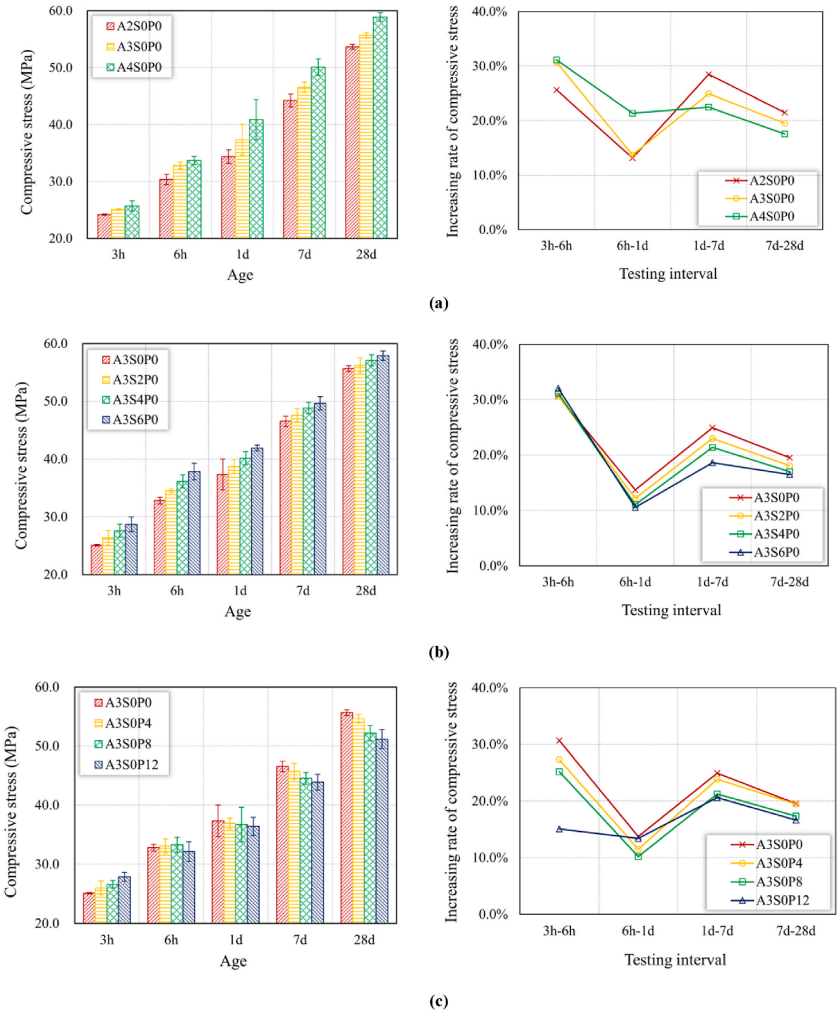


**Fig. 5.** Effects of different components on the compressive strength of HES-ECC with age (a) SAC/FA ratio (b) SF (c) PC.

a distinct transformation on the hydration products of the whole system. It mainly plays an important role in promoting the early strength at the initial period, while SAC contributes more to the strength growth later.

Not only the flexural strength, but also the compressive strength of HES-ECC benefits from the incorporation of SF. The early compressive strength of A3S2P0, A3S4P0 and A3S6P0 at 3 h increased up to 26.4 MPa, 27.6 MPa, and 28.7 MPa, separately. It helps to promote the secondary hydration, filling and densifying the matrix at the same time [30]. However, different from changing SAC/FA ratio, the high-early-strength effect of SF on the compressive strength of HES-ECC mainly acted within 6 h after mixing. The compressive strength of A3S6P0 was 3.6 MPa, 5.1 MPa, 4.6 MPa, 3.1 MPa, and 2.2 MPa higher than that of A3S0P0 at each age, respectively.

### *3.1.3. Effect of PC*

The addition of PC exhibited a similar effect with SF on the flexural strength of HES-ECC. By contrast, addition of SF and PC is more effective on the flexural strength development of HES-ECC during the early stage than increasing SAC/FA ratio. However, the effect of PC is less distinct compared with SF. With the same dosage, SF obtained a higher flexural strength by 0.6 MPa, 0.1 MPa, 1.1 MPa, 0.2 MPa, and 1.0 MPa than PC at each age, respectively.

With regard to A3S0P4, A3S0P8 and A3S0P12, the contribution of PC to the compressive strength of HES-ECC was only limited within 3 h, while loss of compressive strength even happened after that. A higher compressive strength up to 11.16% was obtained at age 3 h with the proportion of PC rising from 0% to 12% with interval 4%. Compared with A3S0P0, the 6 h compressive strength of A3S0P12 was declined by 2.13% while that of A3S0P4 and A3S0P8 were higher. Decrease of compressive strength related to the addition of PC was found in each group in the rest testing ages, among which the compressive strength of A3S0P12 decreased by 0.9 MPa (2.41%), 2.7 MPa (5.79%), and 4.5 MPa (8.08%) than that of A3S0P0, respectively. PC can provide $OH^-$ ions and alkaline environment needed for the reaction of SAC, accelerating the hydration process in the early stage [29]. Nevertheless, given the internal addition method, part of SAC is replaced by PC, of which the proportion is considerable to some extent, triggering the decline of strength later. Comparing three different strategies, it can be found that increasing SAC/FA ratio has little effect on the early compressive

strength, but it is more obvious during the later stage conversely. SF presents exactly the opposite effect, and the compressive strength of A3S6P0 at age 3 h can reach up to 28.7 MPa. Although the addition of PC improves the early compressive strength, it is unfavorable later.

### 3.2. Uniaxial tension tests

Fig. 6 presents the representative stress-strain curves in uniaxial tension tests, and corresponding tensile strength $\sigma_y$ and ultimate tensile strain $\varepsilon_y$ are concluded in Figs. 7 and 8. The tensile strength of all groups developed consistently with age.

#### 3.2.1. Effect of SAC/FA ratio

The increasing rate of uniaxial tensile strength of HES-ECC after 3 h was scarcely influenced by SAC/FA ratio. Compared with the test results at the age of 3 h, the strength growth of A2S0P0, A3S0P0 and A4S0P0 was 1.6 MPa, 1.5 MPa, and 1.6 MPa at age 1d, and was 2.9 MPa, 3.1 MPa, and 2.7 MPa at age 28d, respectively. But similar to the increased flexural strength observed in Section 3.1.1, increasing SAC/FA ratio was also beneficial to the tensile strength. The tensile strength of A3S0P0 and A4S0P0 was 1.76%–5.34% and 6.59%–15.67% higher than that of A2S0P0 at different testing ages, respectively.

Contrary to the development of tensile strength, the ultimate tensile strain of A2S0P0, A3S0P0 and A4S0P0 showed a downward trend over time, with the gradual loss of characteristics of multiple-cracking and strain-hardening. As can be seen from the crack pattern in Fig. 9(a), from 3 h to 1d and then to 28d, the crack number decreases but the crack width and spacing increases. At the beginning of hydration, the matrix strength and the bond strength between matrix and fiber are relatively low. During the process of tension, the cracking strength of the matrix is easy to reach and the fiber can be pulled out from the matrix smoothly. With hydration reaction proceeded, both the matrix strength and the bond strength increase continuously. It leads to the transition of failure mode from fiber pull-out to pull-off, which further results in the decline of ultimate tensile strain [6,38]. In addition, regarding the increased SAC/FA ratio, it also had adverse effects on the ultimate tensile strain. There existed an evident decline in ultimate tensile strain of A3S0P0 by 19.22%, 24.83%, 38.89% compared with A2S0P0, and by 36.84%, 25.51%, 50.74% as to A4S0P0 at different testing ages, separately. Mineral admixture FA is a kind of vitrified microsphere with regular shape. The lubrication effect of FA is weakened with the SAC/FA ratio increased, which makes the fiber hard to pull out and leads to the deterioration of deformation ability eventually [39].

#### 3.2.2. Effect of SF

Distinguished from changing the SAC/FA ratio, by comparing Fig. 7 (a)–(b), it is obvious that the application of a little SF can have a distinct effect on the tensile strength of HES-ECC, particularly at age 3 h. Compared with 3.66 MPa of A3S0P0 at age 3 h, the tensile strength of A3S6P0 could reach 5.59 MPa, increasing by 52.73%. But this also triggered a slowdown as to the growth of later strength. The tensile strength of A3S6P0 only increased by 0.5 MPa and 1.7 MPa at 1d and 28d compared with 3 h, but that of A3S0P0 increased by 1.5 MPa and 3.1 MPa.

The utilization of SF not only improved the tensile strength, but also the ultimate tensile strain. The ultimate tensile strain of A3S2P0, A3S4P0 and A3S6P0 was enhanced by 14.73%, 20.11%, and 23.23% at 3 h compared with A3S0P0, by 72.85%, 73.30%, and 132.58% at 1d, and by 89.70%, 91.52%, and 155.15% at 28d, respectively. SF is constituted by spherical particles with large specific surface area and strong activity [30]. The matrix was densified and the interface between fiber and matrix was optimized, enhancing both the bearing capacity and the deformation capacity of HES-ECC under tension. In addition, the ultimate tensile strain of HES-ECC decreased with age when the dosage of SF was no more than 4%, and there barely existed any difference between the ultimate tensile strain of A3S2P0 and A3S4P0 at each testing age. However, with the dosage of SF further increased to 6%, the ultimate tensile strain of A3S6P0 was improved from 4.35% at 3 h to 5.14% at 1d, and then decreased to 4.21% at 28d, reflecting the lubrication effect of SF thoroughly. Moreover, a more stable deformability at different ages was realized by addition of SF (Fig. 9(b)). The fluctuation value of ultimate tensile strain as to A3S2P0 among different ages was only 0.92%, while that of A3S0P0 reached 1.88%.

#### 3.2.3. Effect of PC

The utilization of PC also helped to enhance the tensile strength of HES-ECC, although it was less effective at age 3 h. The tensile strength was only 5.04 MPa with 12% PC mixed, comparing 5.01 MPa with 2% SF mixed. Nevertheless, as illustrated in Fig. 7 (b)–(c), the superiority of PC reached the peak at 1d, but it remained the same level as that of SF at 28d basically, ranging from 7.01 MPa to 7.31 MPa and from 7.17 MPa to 7.31 MPa for A3S2P0, A3S4P0 and A3S6P0 and A3S0P4, A3S0P8 and A3S0P12 at 28d, separately. It may benefit from the degradation of compressive strength observed at 6 h and later after incorporation of PC, which makes it easier for fibers to pull out and further improve the strain-hardening characteristic. Stress-strain curves of A3S0P4, A3S0P8 and A3S0P12 at 1d in Fig. 6 also present this characteristic, especially for A3S0P12.

The tendency of ultimate tensile strain changing with age after incorporation of PC is similar to that of A3S6P0, which can be described as inverted “V". The ultimate tensile strain of A3S0P4, A3S0P8 and A3S0P12 at 1d was 6.39%, 24.52%, and 17.21% higher compared with that of 3 h, matching the superiority of tensile strength and the characteristic of strain-strengthening after applying PC at 1d. When it comes to 3 h and 28d, the strengthening effect on ultimate tensile strain was not as good as that of SF. The ultimate tensile strain of A3S0P4, A3S0P8 and A3S0P12 was 1.98%–21.81% and 44.85%–80.00% higher than that of A3S0P0 at age 3 h and 28d, while that of A3S2P0, A3S4P0 and A3S6P0 was 14.73%–23.23% and 89.70%–155.15%, respectively. Comparing three different methods, it can be found that increasing SAC/FA ratio can enhance the tensile strength but is unfavorable to the ultimate tensile strain. Both the tensile strength and ultimate tensile strain can benefit from the addition of SF and PC. And HES-ECC mixed with SF even shows a superior deformation ability during the later stage. The ultimate tensile strain of A3S6P0 at age 28d can reach up to

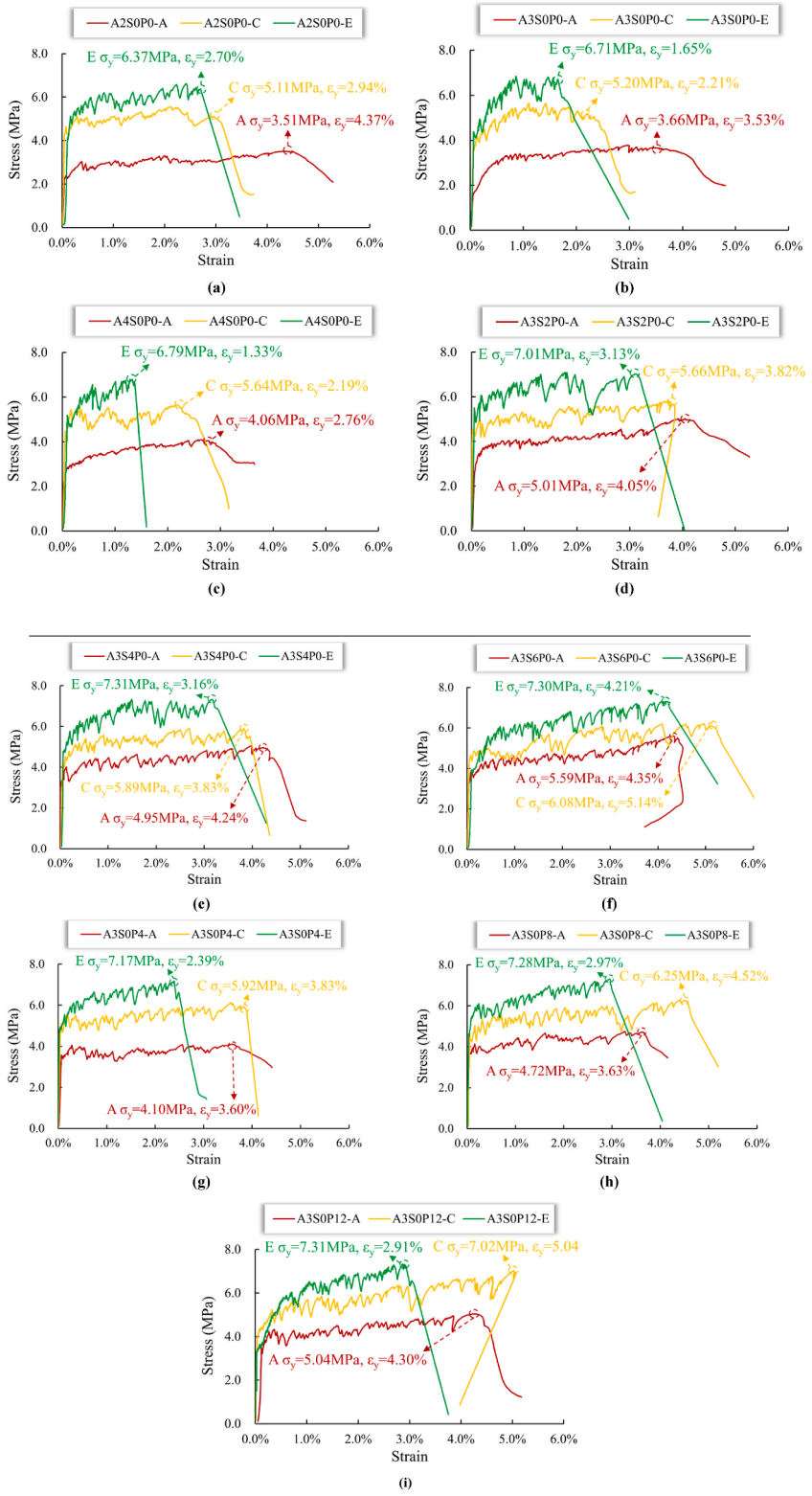


**Fig. 6.** Representative stress-strain curves of HES-ECC in uniaxial tension tests at different testing ages (a) A2S0P0 (b) A3S0P0 (c) A4S0P0 (d) A3S2P0 (e) A3S4P0 (f) A3S6P0 (g) A3S0P4 (h) A3S0P8 (i) A3S0P12.

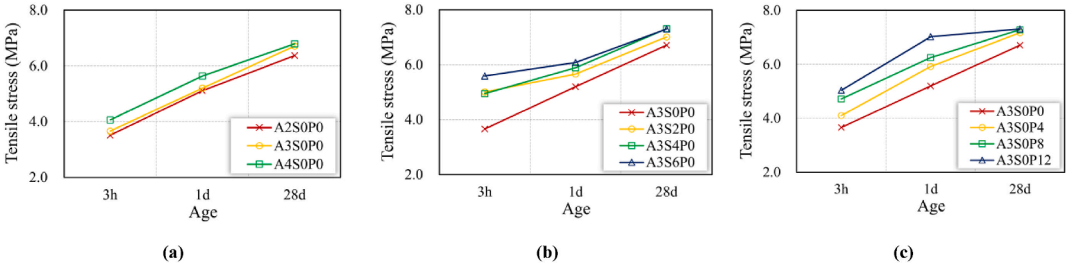


**Fig. 7.** Effects of different components on the tensile strength of HES-ECC with age (a) SAC/FA ratio (b) SF (c) PC.

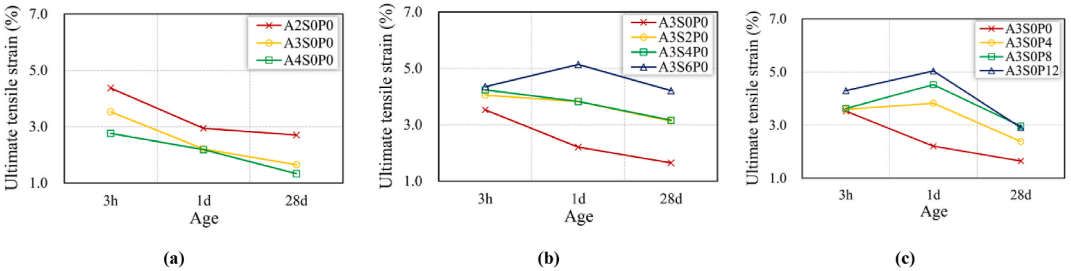


**Fig. 8.** Effects of different components on the ultimate tensile strain of HES-ECC with age (a) SAC/FA ratio (b) SF (c) PC.

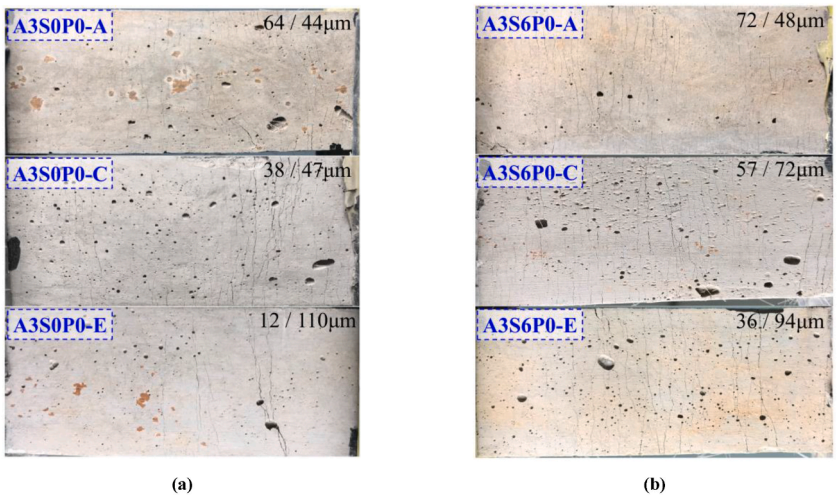


**Fig. 9.** Representative crack development of HES-ECC in uniaxial tension tests (a) A3S0P0 (b) A3S6P0 (The number of crack and the average crack width are marked at the top right.).

4.21%. According to the test results of this study, SF is the most conducive cementitious materials to both the high early-strength and the superior long-term-deformability of HES-ECC. The optimal dosage of SF is recommended to be 6% with SAC/FA ratio remain 3.0.

### *3.3. Interfacial splitting tests*

The roughness and splitting tensile strength of each specimen in the interfacial splitting tests are listed in Table 6. The roughness of all specimens kept approximately the same, and the influence of different interfacial agents on the splitting tensile strength at different ages was investigated. When applying cement paste interfacial agent, the splitting tensile strength was 9.28% higher than that of the unprocessed specimens at age 3 h. Inversely, polymer modified interfacial agent had a negative influence on the splitting tensile strength, with a reduction by 4.12% compared with those without treatment. According to the fracture section of the specimens in splitting tests at age 3 h (Fig. 10), as to the unprocessed specimen, the laitance on the concrete surface was spalled off and adhered to the HES-ECC side. A thin layer of discontinuous laitance could be easily discovered in the middle and lower part of TNIIA-N, even with a small fragment of concrete in the upper left corner. The bond between concrete and HES-ECC mainly consists of mechanical interlocking, chemical adhesive bonding, intermolecular forces (van der Waals force), and fiber bridging effect [18,23]. During the process of tension, the effect of chemical adhesive bonding is dominant while mechanical interlocking can hardly play a role [18]. This phenomenon has already been reflected by specimens without the interfacial agent. The interfacial behavior was further opti-

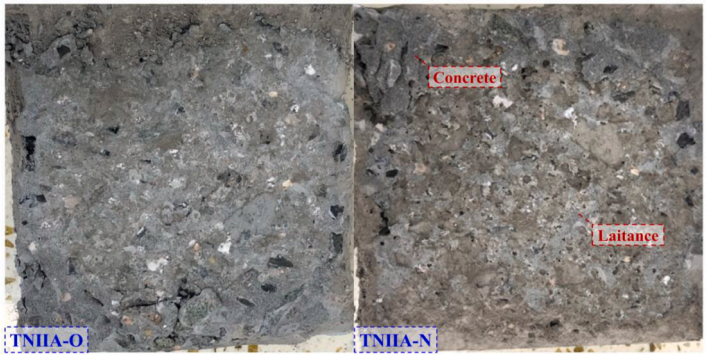


(a)

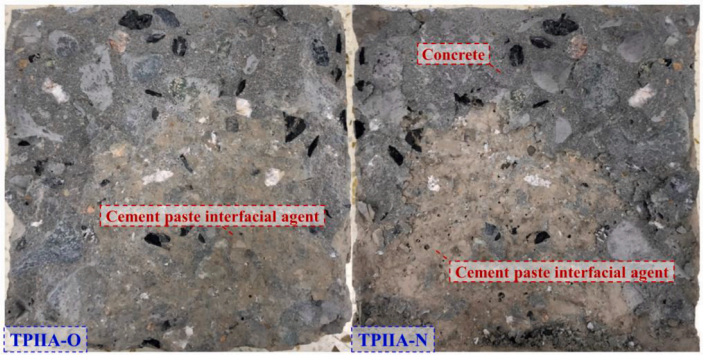


(b)

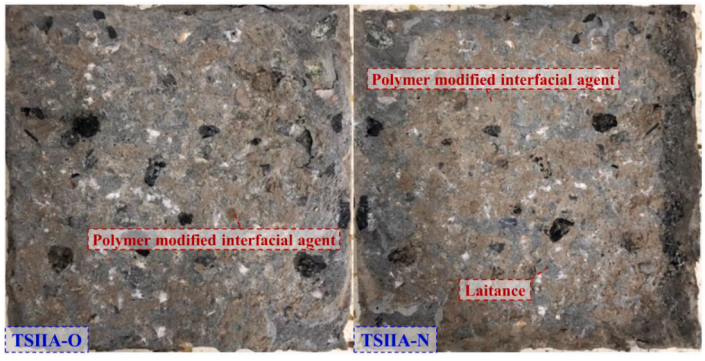


(c)

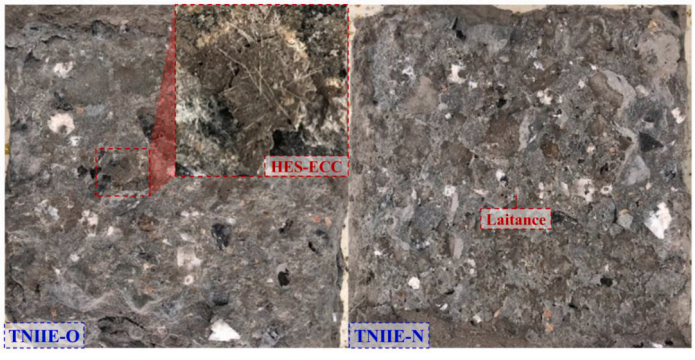


(d)

**Fig. 10.** Section morphology of the interfacial splitting specimens after tests (a) TNIIA (b) TPIIA (c) TSIIA (d) TNIIE ("O" represents the existing concrete side, "N" represents the HES-ECC side).

mized by treating with the cement paste. A large volume of concrete block was observed in the upper half of TPIIA-N, with the fracture interface transferred from the casting interface to the existing concrete side. With regard to the remaining part of TPIIA-N and the corresponding position of TPIIA-O, the brushed interfacial agent was still visible. Interfacial agent can permeate into the existing concrete, increasing the contact area, and filling the voids. Meanwhile, it also enhances the water retention capacity, which promotes the hydration and improves the bonding strength [23]. Wang [19] reported the positive effect of SBR latex modified interfacial agent on the interfacial behaviors between ordinary fiber reinforced cementitious composites and concrete. However, from the test results in this research, SBR latex was incompatible with the cement with high-early-strength. A mass of interfacial agent was found on fracture section TSIIA-O and TSIIA-N, with little laitance adhered to the HES-ECC and without concrete fragment. The early compressive strength of polymer modified interfacial agent was fairly low, taking up only 70.60% of that of cement paste interfacial agent at age 3 h. Besides, brushing the interfacial agent also causes the loss of roughness and the deterioration of fiber bridging effect [23].

The splitting tensile strength of TNII, TPII, and TSII further increased by 26.29%, 26.42%, and 17.74% at age 28d, respectively. As shown in Fig. 10(d), the fracture section of TNIIE-N had a thicker and more continuous laitance layer than that of TNIIA-N, as well as some residual HES-ECC with exposed fibers on TNIIE-O. With regard to TPIIE and TSIIE, section morphology was basically the same as that at age 3d. The failure modes observed in this research is identical to that summarized in the literature, namely interface debonding and concrete fracture [17]. Furthermore, the influence of different interfacial agents on the splitting tensile strength kept unchanged as that at age 3d, that is, the application of cement paste interfacial agent increased the splitting tensile strength by 9.39%, while it was reduced by 10.61% after using the polymer modified interfacial agent. Despite the fact that the strength of polymer modified interfacial agent recovered to the same level as that of the cement paste interfacial agent at age 28d, its contribution to the improvement of bonding properties was still inadequate. Rapid hydration of HES-ECC during the early stage makes it difficult for polymer modified interfacial agent to penetrate and function.

### 3.4. Interfacial direct shear tests

The roughness, relative slip, shear stiffness, and shear strength of each specimen in the interfacial direct shear tests are listed in Table 7, further compared in Fig. 11. The relation curves between direct shear stress and relative slip show an apparent two-stage characteristic, namely, the upward stage and the flat stage. Shear stiffness is defined as the secant stiffness at the turning point between the upward stage and the flat stage as marked in Fig. 12. Fig. 14 exhibits the typical development process of the crack pattern with different interfacial treatment methods obtained by DIC.

As to the chiseled groups without interfacial agents, the relative slip at the flat stage, total relative slip, shear stiffness, and shear strength all showed an ascending trend with the roughness increasing from 0.52 to 2.75. To be specific, compared with the group VNIE with the smoothest interface, the relative slip of VNIIE and VNIIIE at the flat stage was increased by 0.0093 mm and 0.0859 mm, and by 0.0631 mm and 0.1172 mm for the total relative slip, respectively. A rougher interface reduced the brittleness of shear fracture significantly, enhancing the deformation ability in the meantime. Besides, VNIIE and VNIIIE had a higher shear stiffness by up to 21.27%, and a higher shear strength by up to 40.80% compared with VNIE. The increase of roughness directly resulted in the expansion of interfacial contact area, strengthening the adhesive bonding force while enhancing the mechanical interlocking effect [21,23]. As presented in Fig. 13(a), there was merely a thin layer of discontinuous laitance on VNIE-N, and the coarse aggregate in concrete was invisible on VNIE-O. Both existing concrete and post-casting HES-ECC remained intact. VNIIE illustrated the mechanical mutual effect between concrete and HES-ECC intuitively. The surface of VNIIE-N was surrounded by the broken concrete, while there existed a block of HES-ECC in the middle of VNIIE-O. The fiber bridging effect of ECC improved the shear performance during the process of interaction. As to VNIIIE, the fracture section of HES-ECC side was full of broken concrete, of which the coarse aggregate was sheared and the breakage depth was further enlarged.

The roughness of VNIVE with grooved interface was just between VNIE and VNIIE. But its shear properties almost reached the same level as those of VNIIIE. Even if the roughness decreased by 54.18%, the shear strength was only 0.07 MPa lower. Deeper grooves were formed in grooved interface than that by chiseling. Besides, the post-casting HES-ECC was filled to form a whole in local regions, which could be regarded as dowels embedded in the existing concrete. Meanwhile, the excellent deformation ability of ECC guaranteed the sufficient deformation ability of these dowels to prevent the premature failure on the HES-ECC side. Concrete fracture triggered the ultimate failure as shown in VNIVE-N (Fig. 13(d)), and none of broken ECC dowels was observed in VNIVE-O.

With regard to crack development, there were evident differences among different interfacial treatment methods. As shown in Fig. 14 (b), crack initiated on the upper side along the interface of the grooved specimen, of which the corresponding load took up 75.0% of the ultimate load $P_u$. Except local grooves, the rest parts of the grooved interface consist of original smooth surface without any

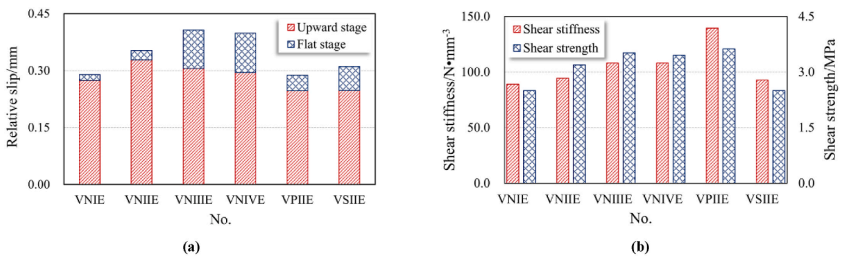


**Fig. 11.** Comparison of the interfacial direct shear tests (a) relative slip (b) shear stiffness and shear strength.

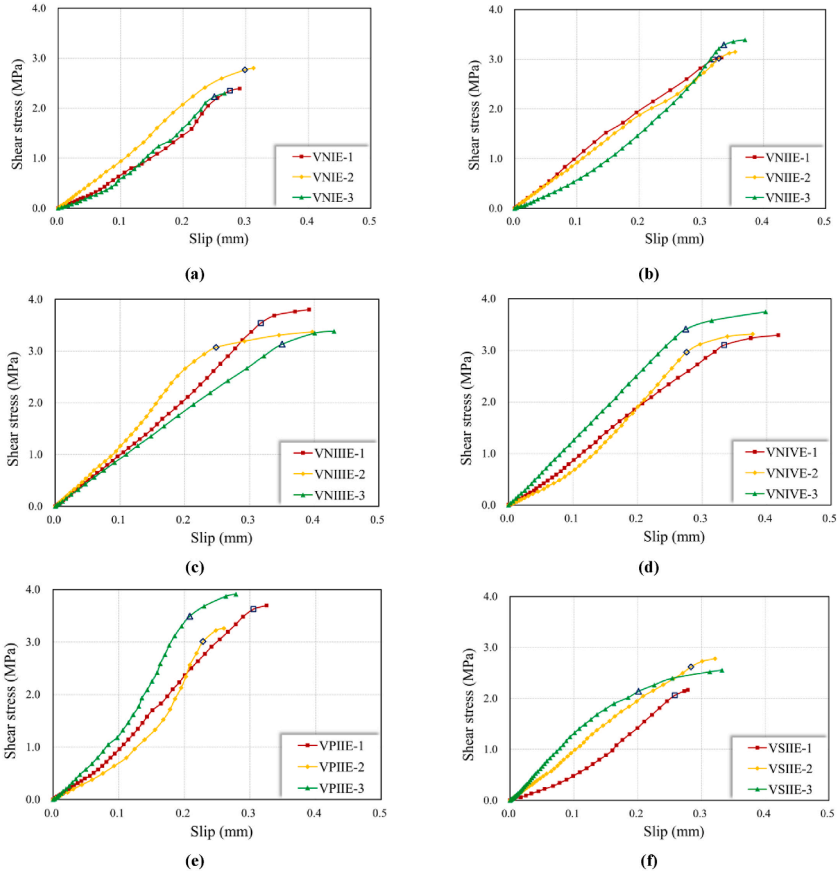


**Fig. 12.** Relationship between direct shear stress and relative slip (a) VNIE (b) VNIIE (c) VNIIIE (d) VNIVE (e) VPIIE (f) VSIIE.

treatment (Fig. 2), which is prone to cracking. Conversely, none of cracks could be found on the chiseled specimen at 75.0% $P_u$ (Fig. 14 (a)), and a small crack was observed in the concrete part far away from the interface at 92.6% $P_u$. The crack of the grooved interface extended to the middle part gradually, with the crack width increasing at the same time. With load reaching 94.2% of the ultimate load, several discontinuous cracks appeared in the middle and lower parts, and the concrete near the grooved interface showed a diagonal crack at 95.1% $P_u$. Then, several cracks extended into the concrete and HES-ECC until failure. The process from initial cracking to ultimate fracture of the specimen with chiseled interface, by contrast, was much shorter. Obvious cracks were generated on the interface at 99.7% $P_u$, as well as a consequent fracture immediately. The cracks barely penetrated into the concrete and HES-ECC, and the continuity of these cracks from concrete to HES-ECC was also reduced.

Influence of the interfacial agents on the direct shear performance is similar to that in the splitting tests. Compared with VNIIE, the shear stiffness and shear strength of VPIIE increased by 47.64% and 13.48% after the cement paste interfacial agent was applied. On the contrary, the total relative slip was decreased by 0.0646 mm, although it presented a more evident shear deformation at the flat stage (Fig. 12 (e)). The fiber bridging effect was restricted and the deformation ability was degraded on account of the barrier of the interfacial agent [23]. It can also be supported by the fracture section in Fig. 13(e). The discontinuous cement paste interfacial agent interweaved with the broken surface layer of concrete in VPIIE-N, and none of broken HES-ECC could be discovered in VPIIE-O. After applying the polymer modified interfacial agent, VSIIE had a 21.63% lower shear strength. The change of relative slip and shear stiffness was not obvious. There existed a large area of polymer modified interfacial agent on the fracture section VSIIE-O and VSIIE-N, while the broken concrete only occupied a small percentage.

It can be found from the interfacial behavior tests that suitable interfacial treatment is indispensable while repair existing concrete structures with HES-ECC. Chiseled interface combined with grooved interface is recommended to bear both the tensile and shear load, respectively. That is, the original smooth surface in the rest parts of grooved interface except local grooves are chiseled. In addition, a thickness of 1–2 mm cement paste interfacial agent is recommended to enhance the interfacial bond strength a step further.

## 4. Conclusions

To realize the effective strengthening and durable repair of concrete structures, HES-ECC featured as both high early-strength and superior long-term-deformability was developed. The influence of SAC/FA ratio, SF, and PC on the high-early-strength and deformation ability of HES-ECC was comprehensively investigated. Moreover, the interfacial behaviors between HES-ECC and existing con-

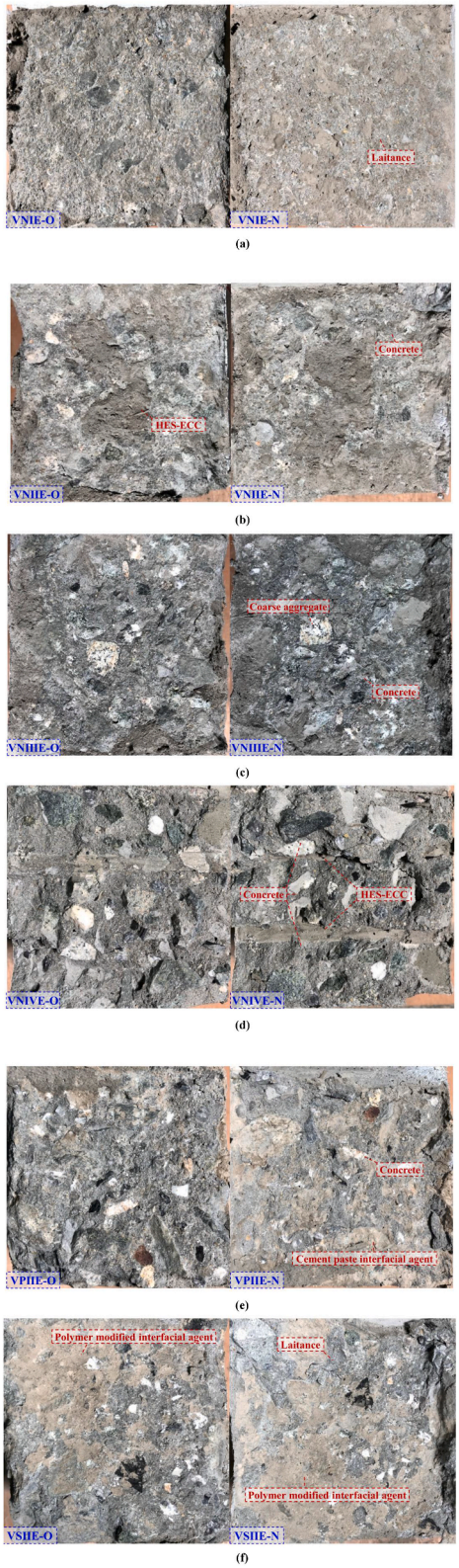


**Fig. 13.** Section morphology of the interfacial direct shear specimens after tests (a) VNIE (b) VNIIE (c) VNIIIE (d) VNIVE (e) VPIIE (f) VSIIE.

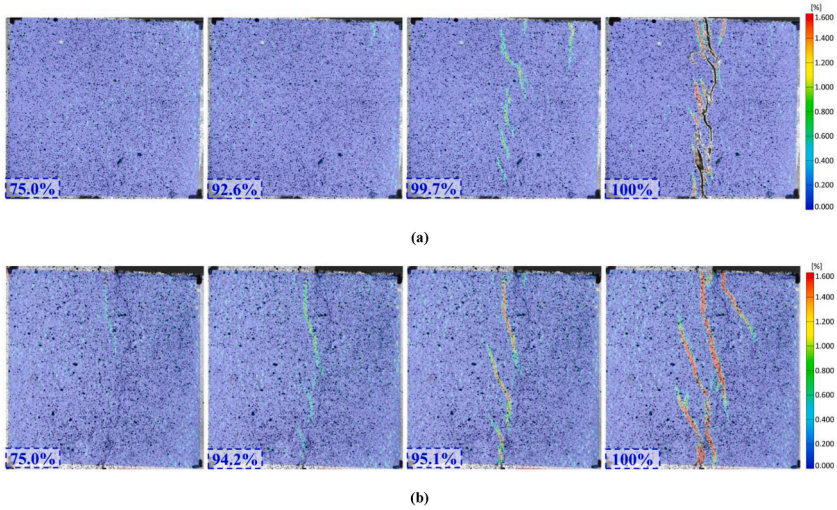


**Fig. 14.** Typical development process of crack pattern in the interfacial direct shear tests (a) Specimen with chiseled interface (VNIIIE) (b) Specimen with grooved interface (VNIVE) (Percentage marked in the figures is the ratio of the corresponding load at each cracking state to the ultimate load $\mathbf{P_u}$).

crete were clarified, with optimal interfacial treatment recommended. Based on the test results, the following conclusions can be drawn:

(1) The high-early-strength effect of SAC/FA ratio, SF, and PC on the flexural strength of HES-ECC could be ranked as SF > PC > SAC/FA ratio. And the high-early-strength effect of SAC/FA ratio, SF, and PC on the compressive strength of HES-ECC peaked at 1d, 6 h, and 3 h, respectively. When the dosage of SF was 6%, the flexural strength of HES-ECC at 3 h could reach 66.67% of that at 28d, and the compressive strength could reach 28.7 MPa. Overused PC is unfavorable to the compressive strength after 3 h.

(2) Increasing SAC/FA ratio enhances the uniaxial tensile strength of HES-ECC but reduces the ultimate tensile strain. Addition of SF and PC can improve both the uniaxial tensile strength and ultimate tensile strain simultaneously. The high-early-strength effect of SF on tensile strength is more efficient, and HES-ECC mixed with SF has a more superior deformation ability. The optimal dosage of SF is recommended to be 6% with SAC/FA ratio remain 3.0. The ultimate tensile strain can reach up to 4.21% at 28d, combining both the high early-strength and the superior long-term-deformability.

(3) Cement paste interfacial agent helps to enhance the chemical adhesive bonding, transferring the fracture interface from the casting interface to the existing concrete side in the splitting tests. The interfacial splitting tensile strength increased by 9.28% and 9.39% at 3 h and 28d compared with those without interfacial agent, respectively. SBR latex is incompatible with the high-early-strength cement. After treating with polymer modified interfacial agent, the splitting tensile strength showed a decline by 4.12% and 10.61% at 3 h and 28d compared with those without interfacial agent, respectively.

(4) The increased roughness of chiseled interface increases the bearing capacity and enhances the deformation ability significantly. Interfacial shear performance of the grooved interface was scarcely deteriorated even if the roughness decreased by 54.18% compared with the chiseled interface. The shear strength was increased by 13.48% with cement paste interfacial agent and decreased by 21.63% with polymer modified interfacial agent. The recommended interfacial treatment is chiseled interface combined with grooved interface, as well as a thickness of 1–2 mm cement paste interfacial agent.

The material design part of this paper failed to consider multiple parameters at the same time. In future studies, the influence of some other mineral admixtures and accelerators should be considered by orthogonal experiments to obtain the HES-ECC with a higher early-strength and a more superior long-term-deformability. As to the interfacial behaviors part, researches on the interfacial behaviors between HES-ECC and existing concrete structures under harsh environments are also indispensable and meaningful.

## Credit author statement

Bo Jiang: Methodology, Experimental tests, and Writing. Zhenxu Qian: Investigation and Reviewing. Dawei Gu: Reviewing and Editing. Jinlong Pan: Conceptualization and Project administration.

## Declaration of competing interest

The authors declare that they have no known competing financial interests or personal relationships that could have appeared to influence the work reported in this paper.

## Data availability

Data will be made available on request.

## Acknowledgements

This work was financially supported by the Carbon Emission Peak and Carbon Neutrality Innovative Science Foundation of Jiangsu Province (No. BE2022606) and Victoria-Jiangsu Innovation and Technology R&D Fund (BZ2020019).

## References

[1] A.M. Neville, Properties of Concrete, Pearson Education Limited, 2011.
[2] R.K.L. Su, Y. Zhang, A novel elastic-body-rotation model for concrete cover spalling caused by non-uniform corrosion of reinforcement, Construct. Build. Mater. 213 (2019) 549–560, https://doi.org/10.1016/j.conbuildmat.2019.04.096.
[3] H. Fakhri, K.A. Ragalwar, R. Ranade, On the use of Strain-Hardening Cementitious Composite covers to mitigate corrosion in reinforced concrete structures, Construct. Build. Mater. 224 (2019) 850–862, https://doi.org/10.1016/j.conbuildmat.2019.07.052.
[4] P.H. Emmons, D.J. Sordyl, The state of the concrete repair industry, and a vision for its future, Concr. Repair Bull. (2006) 7–14.
[5] D.R. Morgan, Compatibility of concrete repair materials and systems, Construct. Build. Mater. 10 (1996) 57–67, https://doi.org/10.1016/0950-0618(95)00060-7.
[6] S. Wang, V.C. Li, High-early-strength engineered cementitious composites, ACI Mater. J. 103 (2006) 97–105, https://doi.org/10.14359/15260.
[7] B. Wang, S. Xu, F. Liu, Evaluation of tensile bonding strength between UHTCC repair materials and concrete substrate, Construct. Build. Mater. 112 (2016) 595–606, https://doi.org/10.1016/j.conbuildmat.2016.02.149.
[8] F. Saucier, Durabilité de l'adhérence des réparations en béton, Laval University, 1991.
[9] M.H. Fiebrich, Scientific aspects of adhesion phenomena in the interface mineral substrate-polymers, in: F.H. Wittman (Ed.), Adherence of Young and Old Concrete, Proceedings of 2nd Bolomey Workshop, Aedificatio Verlag, Unterengstringen, 1994.
[10] H.R. Sasse, M. Fiebrich, Bonding of polymer materials to concrete, Mater. Construcción 16 (1983) 293–301, https://doi.org/10.1007/BF02473695.
[11] M. Li, V.C. Li, Behavior of ECC-concrete layered repair system under drying shrinkage conditions, Restor. Build. Monum. 12 (2006) 143–160, https://doi.org/10.1515/rbm-2006-6040.
[12] C.K.Y. Leung, V.C. Li, Effect of fiber inclination on crack bridging stress in brittle fiber reinforced brittle matrix composites, J. Mech. Phys. Solid. 40 (1992) 1333–1362, https://doi.org/10.1016/0022-5096(92)90018-W.
[13] V.C. Li, C.K.Y. Leung, Steady-state and multiple cracking of short random fiber composites, J. Eng. Mech. 118 (1992) 2246–2264, https://doi.org/10.1061/(ASCE)0733-9399(1992)118:11(2246).
[14] V.C. Li, Engineered Cementitious Composites (ECC), Springer-Verlag GmbH Germany, 2019, https://doi.org/10.1007/978-3-662-58438-5.
[15] M. Qasim, C.K. Lee, Y.X. Zhang, An experimental study on interfacial bond strength between hybrid engineered cementitious composite and concrete, Construct. Build. Mater. 356 (2022) 129299, https://doi.org/10.1016/j.conbuildmat.2022.129299.
[16] F. Yuan, J.L. Pan, L.T. Dong, C.K.Y. Leung, Mechanical behaviors of steel reinforced ECC or ECC/concrete composite beams under reversed cyclic loading, J. Mater. Civ. Eng. 26 (2014) 04014047, https://doi.org/10.1061/(ASCE)MT.1943-5533.0000935.
[17] J. Tian, X. Wu, W.W. Wang, S. Hu, X. Tan, Y. Du, Y. Zheng, C. Sun, Experimental study and mechanics model of ECC-to-concrete bond interface under tensile loading, Compos. Struct. 285 (2022) 115203, https://doi.org/10.1016/j.compstruct.2022.115203.
[18] J. Tian, X. Wu, Y. Zheng, S. Hu, Y. Du, W. Wang, C. Sun, L. Zhang, Investigation of interface shear properties and mechanical model between ECC and concrete, Construct. Build. Mater. 223 (2019) 12–27, https://doi.org/10.1016/j.conbuildmat.2019.06.188.
[19] B. Wang, Q. Li, F. Liu, J. Wang, S. Xu, Shear bond assessment of UHTCC repair using push-out test, Construct. Build. Mater. 164 (2018) 206–216, https://doi.org/10.1016/j.conbuildmat.2017.12.148.
[20] S. Xu, F. Mu, J. Wang, W. Li, Experimental study on the interface behavior between sprayed UHTCC and concrete substrate, Construct. Build. Mater. 195 (2019) 638–649, https://doi.org/10.1016/j.conbuildmat.2018.11.102.
[21] B.A. Tayeh, B.H. Abu Bakar, M.A. Megat Johari, Y.L. Voo, Mechanical and permeability properties of the interface between normal concrete substrate and ultra high performance fiber concrete overlay, Construct. Build. Mater. 36 (2012) 538–548, https://doi.org/10.1016/j.conbuildmat.2012.06.013.
[22] M. Sahmaran, H.E. Yücel, G. Yildirim, M. Al-Emam, M. Lachemi, Investigation of the bond between concrete substrate and ECC overlays, J. Mater. Civ. Eng. 26 (2014) 167–174, https://doi.org/10.1061/(asce)mt.1943-5533.0000805.
[23] X. Shang, F. Xu, J. Yu, L. Li, Z. Lu, Study on the interfacial shear performance between engineered cementitious composites and concrete after being subjected to high temperatures, J. Build. Eng. 44 (2021) 103328, https://doi.org/10.1016/j.jobe.2021.103328.
[24] S. Gao, X. Zhao, J. Qiao, Y. Guo, G. Hu, Study on the bonding properties of Engineered Cementitious Composites (ECC) and existing concrete exposed to high temperature, Construct. Build. Mater. 196 (2019) 330–344, https://doi.org/10.1016/j.conbuildmat.2018.11.136.
[25] X. Wu, J. Tian, H. Ma, Y. Zheng, S. Hu, W. Wang, Y. Du, W. Huang, C. Sun, Z. Zhu, Investigation on interface fracture properties and nonlinear fracture model between ECC and concrete subjected to salt freeze-thaw cycles, Construct. Build. Mater. 259 (2020) 119785, https://doi.org/10.1016/j.conbuildmat.2020.119785.
[26] S. Gao, J. Jin, G. Hu, L. Qi, Experimental investigation of the interface bond properties between SHCC and concrete under sulfate attack, Construct. Build. Mater. 217 (2019) 651–663, https://doi.org/10.1016/j.conbuildmat.2019.05.121.
[27] H. Ma, S. Qian, Z. Zhang, Effect of self-healing on water permeability and mechanical property of Medium-Early-Strength Engineered Cementitious Composites, Construct. Build. Mater. 68 (2014) 92–101, https://doi.org/10.1016/j.conbuildmat.2014.05.065.
[28] M. Li, V.C. Li, High-early-strength engineered cementitious composites for fast, durable concrete repair-material properties, ACI Mater. J. 108 (2011) 3–12, https://doi.org/10.14359/51664210.
[29] M. Şahmaran, M. Al-Emam, G. Yıldırım, Y.E. Simsek, T.K. Erdem, M. Lachemi, High-early-strength ductile cementitious composites with characteristics of low early-age shrinkage for repair of infrastructures, Mater. Struct. 48 (2015) 1389–1403, https://doi.org/10.1617/s11527-013-0241-z.
[30] H. Deng, Utilization of local ingredients for the production of high-early-strength engineered cementitious composites, Adv. Mater. Sci. Eng. 2018 (2018), https://doi.org/10.1155/2018/8159869.
[31] G. Yıldırım, M. Sahmaran, M.K.M. Al-Emam, R.K.H. Hameed, Y. Al-Najjar, M. Lachemi, Effects of compressive strength, autogenous shrinkage, and testing methods on bond behavior of high-early- strength engineered cementitious composites, ACI Mater. J. 112 (2015) 409–418.
[32] J. Zhang, C. Gong, Z. Guo, M. Zhang, Engineered cementitious composite with characteristic of low drying shrinkage, Cement Concr. Res. 39 (2009) 303–312, https://doi.org/10.1016/j.cemconres.2008.11.012.
[33] Standard for Test Methods of Concrete Physical and Mechanical Properties (GB/T 50081-2019), China Architecture & Building Press, 2019.
[34] Method of Testing Cements-Determination of Strength (GB/T 17671-1999 (Idt ISO 679:1989)), China Architecture & Building Press, 1999.
[35] Standard for Test Method of Performance on Building Mortar (JGJ/T 70-2009), China Architecture & Building Press, 2009.
[36] Recommendations for Design and Construction of High Performance Fiber Reinforced Cement Composites with Multiple Fine Cracks, Japan Society of Civil Engineers, 2008.
[37] A.K.F. Cheung, C.K.Y. Leung, Shrinkage reduction of high strength fiber reinforced cementitious composites (HSFRCC) with various water-to-binder ratios, Cem. Concr. Compos. 33 (2011) 661–667, https://doi.org/10.1016/j.cemconcomp.2011.03.009.
[38] S. Gao, Z. Wang, W. Wang, H. Qiu, Effect of shrinkage-reducing admixture and expansive agent on mechanical properties and drying shrinkage of Engineered Cementitious Composite (ECC), Construct. Build. Mater. 179 (2018) 172–185, https://doi.org/10.1016/j.conbuildmat.2018.05.203.
[39] S.X. Wang, V.C. Li, Engineered cementitious composites with high-volume fly ash, ACI Mater. J. 104 (2007) 233–241.